



Article

Processing of the Ti25Ta25Nb3Sn Experimental Alloy Using ECAP Process for Biomedical Applications

Celso Bortolini, Jr.¹ , João Pedro Aquiles Carobolante¹, Ilana Timokhina², Angelo Caporalli Filho¹ and Ana Paula Rosifini Alves^{1,*}

¹ Department of Materials and Technology, School of Engineering and Sciences, São Paulo State University (Unesp), Guaratinguetá Campus, Guaratinguetá, São Paulo 12516-410, Brazil; celso.bortolini@unesp.br (C.B.J.); pedro.carobolante@unesp.br (J.P.A.C.); angelo.caporalli@unesp.br (A.C.F.)

² Institute for Frontier Materials, Deakin University, Waurn Ponds Campus, Geelong 3217, Australia; ilana.timokhina@deakin.edu.au

* Correspondence: paula.rosifini@unesp.br

Abstract: The development of titanium- β alloys for biomedical applications is associated with the addition of alloying elements or the use of processing techniques to obtain suitable bulk properties. The Ti25Ta25Nb3Sn alloy has been highlighted for its mechanical properties and biocompatibility. To further enhance the properties of titanium alloys for biomedical applications, equal channel angular pressing (ECAP) was used due to its capability of refining the microstructure of the alloy, leading to improved mechanical properties without significant changes in Young's modulus. This study aims to evaluate the impact of ECAP on the microstructure of the Ti-25Sn-25Nb-3Nb alloy and investigate the correlation between the microstructure, mechanical properties, and corrosive behavior. Grain refinement was achieved after four ECAP passes, with an average grain diameter of 395 nm and a non-homogeneous structure, and microhardness was slightly increased from 193 to 212 HV after four ECAP passes. The thermomechanical aspects of the ECAP processing have led to the formation of a metastable α'' phase during the first two passes, while after four passes, the structure was composed only of the β phase. The corrosion resistance of the alloy was increased after four passes, presenting the best results in terms of the improvement of passivation corrosion density.

Keywords: titanium alloys; biomaterials; ECAP; mechanical processing



Citation: Bortolini, C., Jr.; Carobolante, J.P.A.; Timokhina, I.; Caporalli Filho, A.; Rosifini Alves, A.P. Processing of the Ti25Ta25Nb3Sn Experimental Alloy Using ECAP Process for Biomedical Applications. *J. Manuf. Mater. Process.* **2023**, *7*, 201. <https://doi.org/10.3390/jmmp7060201>

Academic Editors: Chetan P. Nikhare and William J. Emblom

Received: 9 October 2023

Revised: 7 November 2023

Accepted: 8 November 2023

Published: 10 November 2023



Copyright: © 2023 by the authors. Licensee MDPI, Basel, Switzerland. This article is an open access article distributed under the terms and conditions of the Creative Commons Attribution (CC BY) license (<https://creativecommons.org/licenses/by/4.0/>).

1. Introduction

Since the 1960s, the use of titanium alloys in biomedical applications has increased due to their mechanical properties and excellent biocompatibility. Although the Ti-6Al-4V alloy is the most commercially used, issues related to its biocompatibility in permanent applications, with Al and V associated with Alzheimer's and allergic diseases, respectively, and its interaction with bone tissue due to its high Young's modulus, have motivated the search for new Ti-based alloys [1–4].

In this context, systems composed of beta-stabilizing alloy elements such as Ta and Nb have been highlighted, mainly due to their good results related to Young's modulus. A low modulus, closer to those found in bone tissue, reduces the stress shielding effect and improves cohesion at the bone-implant interface [5,6]. In addition, some of the beta-stabilizing elements also exhibit high corrosion resistance due to the formation of stable oxides, contributing to the passivation of the alloys and consequently improving biocompatibility. These results have led to an increased interest in studies in this area. Some promising alloys developed recently include: Ti-Mo-Nb [4,7,8], Ti-Mo-Nb-Zr [3,9], Ti-Nb-Cu [10], Ti-Zr-Nb [11], Ti-Nb-Sn [12], Ti-Nb-Ta [13,14], Ti-Nb-Zr-Mn-Sn [15], Ti-Mo-Nb-O [16], Ti-Nb-Zr-Ta [16], Ti-Nb-Zr-Ta-Sn [1], and Ti-Ta-Nb-Sn [17,18].

Tantalum is a beta-phase stabilizer with high biocompatibility and corrosion resistance due to the formation of a Ti_2O_5 layer on its surface. Previous studies by Zhou (2004) eval-

ated the ultimate tensile strength (UTS) and Young's modulus for the Ti-Ta system, in which Ti-30Ta and Ti-70Ta alloys showed low elasticity modulus, 69 and 67 GPa, respectively, and UTS of 590 MPa [19]. Niobium is also a beta-phase stabilizer, and it presents high biocompatibility and corrosion resistance superior to Ti. In binary Ti systems, an increase in toughness, UTS, shape memory, and superelasticity effects have been reported due to the presence of martensitic phases [20]. Bertrand (2010; 2013) reported that the Ti-25Ta-25Nb ternary alloy presented a monophase structure (beta-phase) and excellent biocompatibility with low Young's modulus [21,22]. However, the presence of the martensitic phase was also observed, causing the double-yielding phenomenon, which may be detrimental to the development of implants for bone tissue due to the high probability of fracture [23]. Tin has shown satisfactory results in terms of biocompatibility and has been employed in biodegradable alloys with Mg and Zn, as well as in Ti alloys with Ta, Nb, and Zr, among others [24,25]. The Ti-Nb-Sn and Ti-Nb-Zr-Ta-Sn systems provide better biocompatibility, lower Young's modulus, and higher mechanical strength and ductility compared to grade 2 titanium and Ti-6Al-4V alloy [1,25,26].

The addition of Sn to the Ti-25Ta-25Nb alloy was evaluated by Seixas (2018) and Silva (2023), and the authors reported an increase in mechanical strength and a decrease in Young's modulus [17,18]. The Ti25Ta25Nb3Sn alloy presented a UTS of 583 MPa, hardness of 193 HV, and modulus of 65 GPa, while the Ti-25Ta-25Nb-5Sn alloy presented a modulus of 85 GPa and hardness of 198 HV, more suitable results for biomedical applications in bone tissue compared to Ti-6Al-4V alloy, which has Young's modulus of 110 GPa and hardness of 184 HV. The addition of Sn also inhibited the double-yielding phenomenon and presented good corrosive behavior, although an increase in grain size was verified when compared to the Ti25Ta25Nb alloy.

Due to the metastability of the β phase, the microstructure of β -titanium alloys cannot be changed by heat treatments so the use of mechanical processing can also contribute to grain refinement [8]. Equal channel angular pressing (ECAP) is a processing technique capable of modifying the alloy's microstructure through severe mechanical deformation, resulting in grain size reduction. Microstructure refinement contributes to the increase in mechanical properties, such as hardness, yield, and fatigue strength. Furthermore, ECAP has little interference with the material structure, resulting in small or no changes in Young's modulus. These characteristics are interesting for materials developed for use in bone implants. In addition to modifying mechanical properties, microstructure refinement also affects other material properties, such as surface chemical activity, due to a higher defect density, which can result in a better corrosive behavior of the alloy [9,27].

To continue the group's previous study, the purpose of the present research was to evaluate the influence of ECAP (two and four passes) on the microstructure of the Ti-25Sn-25Nb-3Nb alloy, as well as to investigate the correlation between the microstructure, the mechanical properties, and the corrosive behavior of the alloy to establish the Ti25Ta25Nb3Sn alloy as a potential material for biomedical applications.

2. Materials and Methods

The Ti-25Ta-25Nb-3Sn experimental alloy was obtained from sheets of titanium (grade 2), tantalum (99.99%), niobium (99.99%), and tin (99.99%). The methodology used in the processing was based on our previous studies with this alloy [14,17,18]. During melting, ingots were melted and re-melted at least ten times due to the difference between the melting point of these materials. The ingots were homogenized in a vacuum furnace at 950 °C for 24 h to eliminate any residual chemical segregation, and worked into bars with a 10 mm diameter via cold swaging. To stabilize the β phase, the bars were solution-treated in a vacuum furnace at 900 °C for 2 h followed by water quenching. Warm ECAP was added to the already studied processing route [14,17,18] to change the grain size of the alloy.

The bars were cut into 40 mm length samples and subjected to ECAP via route Bc at 773 K in an L-shaped split-die with an internal channel angle, Φ , of 90° and an outer arc of curvature, Ψ , of 20.6°, as shown on Figure 1. In this study, the samples were subjected to

two and four ECAP passes. According to the literature, in order to produce a homogeneous nanostructure, most materials need at least four ECAP passes [28–31]. After two passes, longitudinal and cross-section samples were cut from the ECAPed billet, and after four passes, samples were cut from the cross-section.

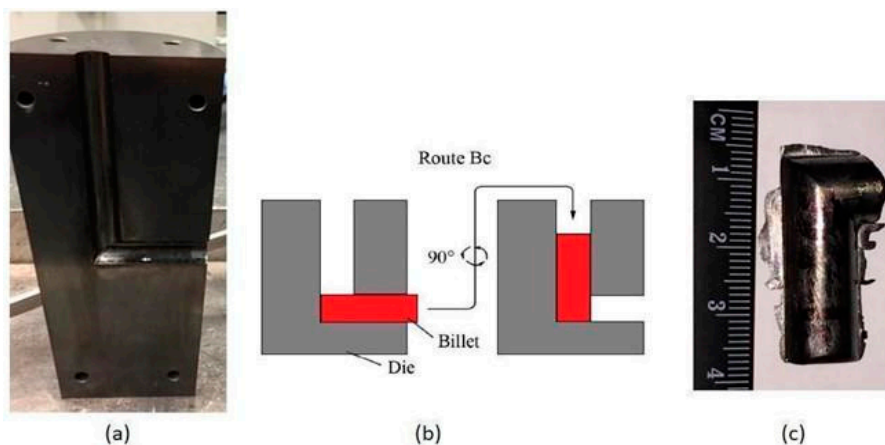


Figure 1. (a) Die used for processing; (b) schematic representation of ECAP processing; (c) ingot after ECAP processing (4 passes).

Microstructural analysis was carried out after ECAP using Scanning Electron Microscopy (SEM), Electron Backscatter Diffraction (EBSD), and X Ray Diffraction (XRD). The samples were ground with sandpaper of grit sizes varying between 220 and 4000 and polished with a solution composed of colloidal Silica and H₂O₂. The SEM imaging was carried out using a Zeiss Supra 55VP FEG-SEM and performed at 20kV and 10 mm working distance. The anisotropy and grain size of the alloy after ECAP were evaluated using EBSD and XRD analysis. EBSD data collection was conducted in a Zeiss LEO 1530 FEG-SEM equipped with an EBSD Detector in the same samples used for SEM. The acquisition was performed at 20 kV, 10 mm working distance, a tilt angle of 70°, and a scan step of 0.05 μm . XRD data collection was carried out in a Brüker D8 Advance Eco X-Ray Diffractometer with a Lynxeye XE-T ODC 1D detector, using 40 kV, 25 mA with a fixed time of 1.6 s, and a step of 0.02°.

Microhardness tests were carried out with the same samples which had been previously used for microstructural characterization. Vickers microhardness was measured with a Shimadzu model HMV 2T microdurometer and conducted with a load of 1.961 N for 15 s.

Also, a study was conducted to evaluate the corrosive behavior of Ti-25Ta-25Nb-3Sn alloy using open circuit potential (OCP) and potentiodynamic polarization tests. Three alloy-processing conditions were analyzed: the Ti-25Ta-25Nb-3Sn alloy before ECAP, and after ECAP technique with 2 (Ti-25Ta-25Nb-3Sn ECAP-2) and 4 (Ti-25Ta-25Nb-3Sn ECAP-4) passes. In all cases analyzed, samples were taken from the cross-section of the ingot produced. The tests were performed in a fluorinated physiological medium composed of 0.15 M NaCl and 0.03 M NaF, at a temperature of 37 °C (± 0.5 °C) and pH of 6.0. A conventional three-electrode cell was employed containing a platinum electrode as the counter electrode and a saturated calomel electrode (SCE) as the reference electrode. The alloy discs with a diameter of 10 mm and thickness of 3 mm were used as the working electrode, positioned on a sample holder with an exposed area of approximately 0.8 cm^2 . OCP and potentiodynamic polarization measurements were performed in triplicate for each condition analyzed. The tests were conducted in sequence: initially, OCP data were collected for 10.8 ks after immersing the samples in the fluorinated solution. Then, potentiodynamic polarization tests were initiated, with a potential range swept from −0.3 V against OCP to +3.0 V, at a scan rate of 1 mV/s. The Tafel method was used to obtain the corrosion potential (Ecorr) and corrosion current density (Jcorr), and the parameters were obtained using the Tafel Extrapolation application available in OriginPro 2016 software.

(OriginLab Corporation, Northampton, MA, USA). The passivation current density (J_p) was also obtained.

3. Results and Discussion

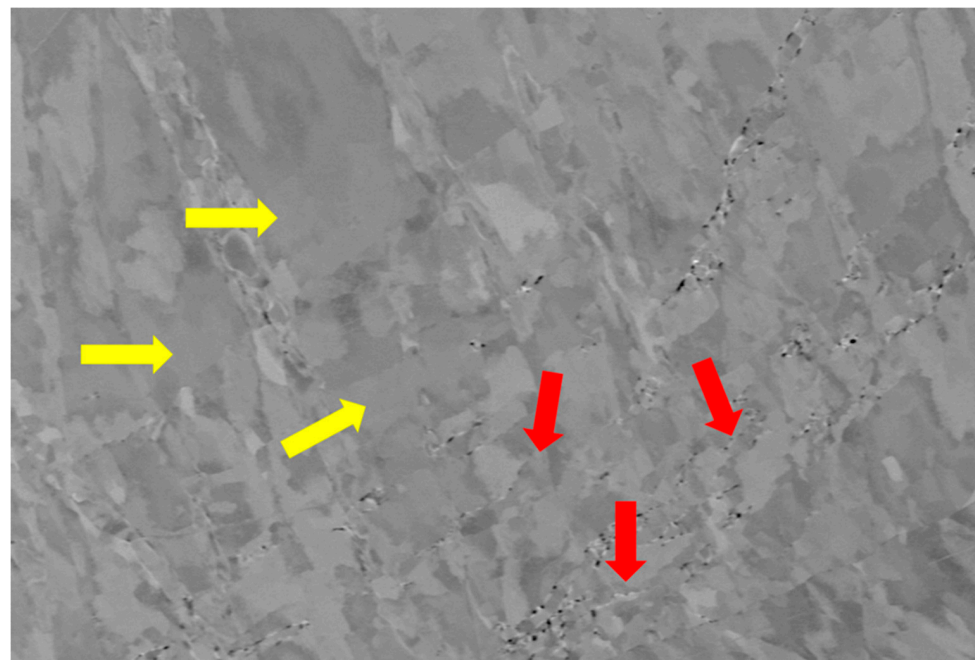
According to the results of our group's previous studies, the average grain size of the β -phased Ti-25Ta-25Nb-3Sn alloy before ECAP processing is 700 μm [17].

The microstructure after two passes (Ti-25Ta-25Nb-3Sn ECAP-2) showed a distribution of fine grains with elongated coarse grain areas, indicating the start of the grain refinement process (Figure 2a,b). The cross-section microstructure of the Ti-25Ta-25Nb-3Sn after two passes can be seen in Figure 2a, where a microstructure consisting of coarse and fine grains is observed, with the red arrows indicating the distribution of fine grains and the yellow arrows indicating the elongated coarse grains. Similarly, the longitudinal section microstructure of the Ti-25Ta-25Nb-3Sn after two passes is shown in Figure 2b, with the same indication of a fine-grained structure (red arrows) inside an elongated coarse grain structure (yellow arrows) matching the distribution observed in the cross-section.

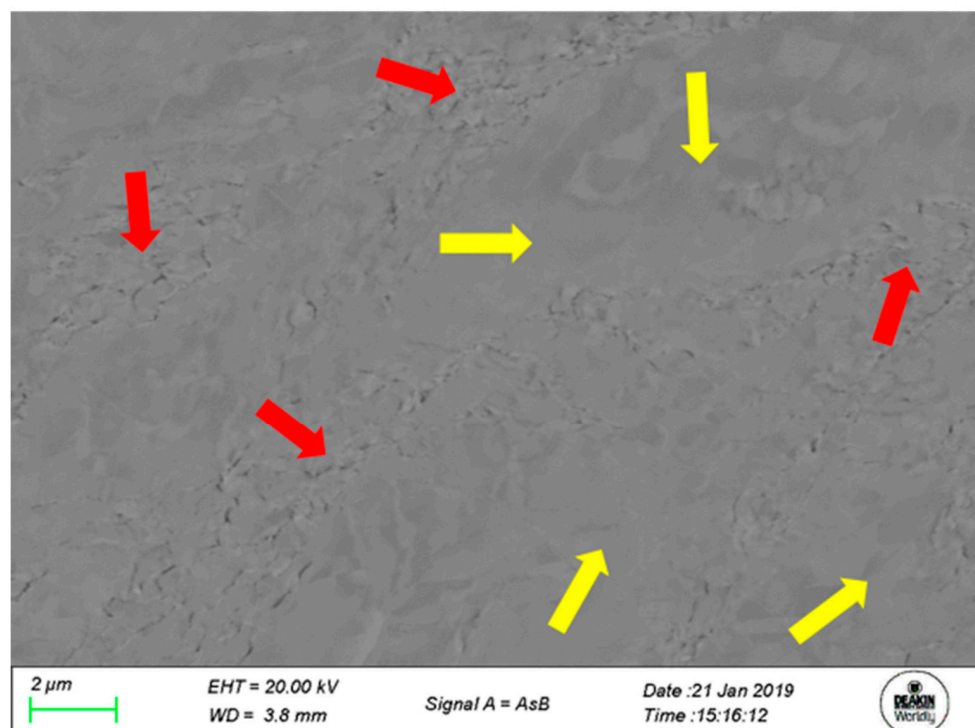
From EBSD maps (Figures 3a and 4a) it was possible to observe the same distribution of fine grains inside the elongated coarse grain areas, as seen in the SEM images. The EBSD map of the Ti-25Ta-25Nb-3Sn after two ECAP passes and the inverse pole figure of the cross-section and the longitudinal section are shown in Figures 3 and 4, respectively. The results obtained after two passes confirm the hypothesis that more ECAP passes are needed to produce a homogeneous fine-grained microstructure.

After four ECAP passes (Ti-25Ta-25Nb-3Sn ECAP-4) the elongated coarse structure is not present anymore; the SEM image of the cross-section microstructure can be seen in Figure 5a and shows only a fine grain distribution, with an average grain diameter of 395 nm (± 143), although the grain refinement imposed by the ECAP process was not enough to produce a homogeneous structure, as indicated by the high standard deviation of average grain diameter. The change in the structure was confirmed by the EBSD map of the cross-section, as can be seen in Figure 5b. According to the inverse pole figures, the crystallographic orientation after two ECAP passes was distributed along the [111] plane (Figures 3b and 4b), while after four ECAP passes, the crystallographic orientation was distributed between the [101] and [001] planes (Figure 5c). Despite the insufficient reduction in grain size, a reduction in the anisotropy can be observed due to the change in the growth orientation. Similar results were observed by Gunderov et al. (2013) [28]. While studying the influence of the ECAP processing on the structure of commercially pure Ti, the authors used a 120° die and a processing temperature of 200 °C; after four ECAP passes, the average grain diameter was 300 nm but the structure was not homogeneous. After eight ECAP passes, the average grain diameter was approximately 200 nm and the authors observed a homogeneity on the structure. Polyakov et al. (2014) evaluated the evolution of the microstructure of the Ti6Al4V after ECAP processing using a 120° die, following the Bc route and with a processing temperature of 600 °C. The authors observed that after four ECAP passes, the average grain diameter was reduced from 15 μm to approximately 240 nm [29]. Terynková et al. (2018) studied the microstructure and mechanical properties of the Ti15Mo alloy after ECAP processing using a 120° die and 250 °C processing temperature, observing an ultrafine-grained structure after four ECAP passes; the EBSD showed that the twinning plane was [112] [30]. The microstructure of the Ti13Nb13Zr after ECAP was investigated by Xu et al. (2023); the samples were subjected to one ECAP pass using a 90° die, resulting in a structure with an average grain size of 152.79 nm. The authors observed the formation of a martensitic α' phase before the ECAP processing, which partially decomposed into α and β phases during the ECAP processing [32]. The formation of an ultrafine-grained structure was reported by Munir et al. (2022) when studying the Ti28Nb35.4Zr alloy submitted to the ECAP processing, with an increase of 23% in Vickers hardness from 244 to 299 HV [33]. Likewise, Valiev et al. (2020) evaluated the structure and mechanical properties of NiTi with the shape memory effect

processed by ECAP, and observed the formation of an ultrafine-grained structure with an average grain size of about 200 nm [34].



(a)



(b)

Figure 2. SEM Images of the Ti-25Ta-25Nb-3Sn alloys after 2 ECAP passes showing the distribution of a fine-grained structure (red arrows) with a coarse-grained area (yellow arrows) for the (a) cross-section and (b) longitudinal section.

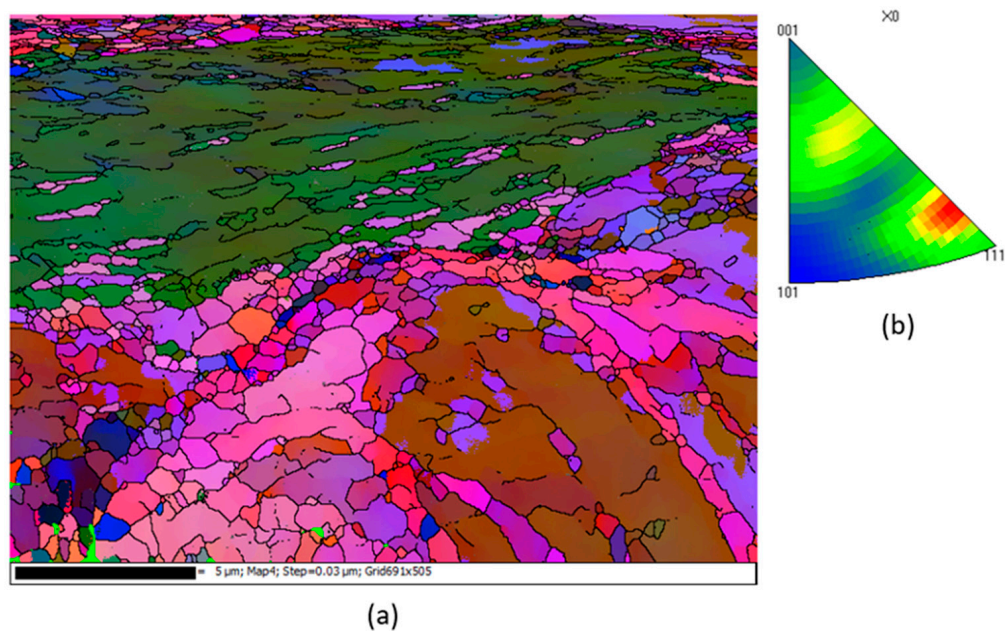


Figure 3. EBSD map of the cross-section of the Ti-25Ta-25Nb-3Sn alloy after 2 ECAP passes showing (a) an elongated coarse grain with a fine grain distribution area and (b) the inverse pole figure of the same region.

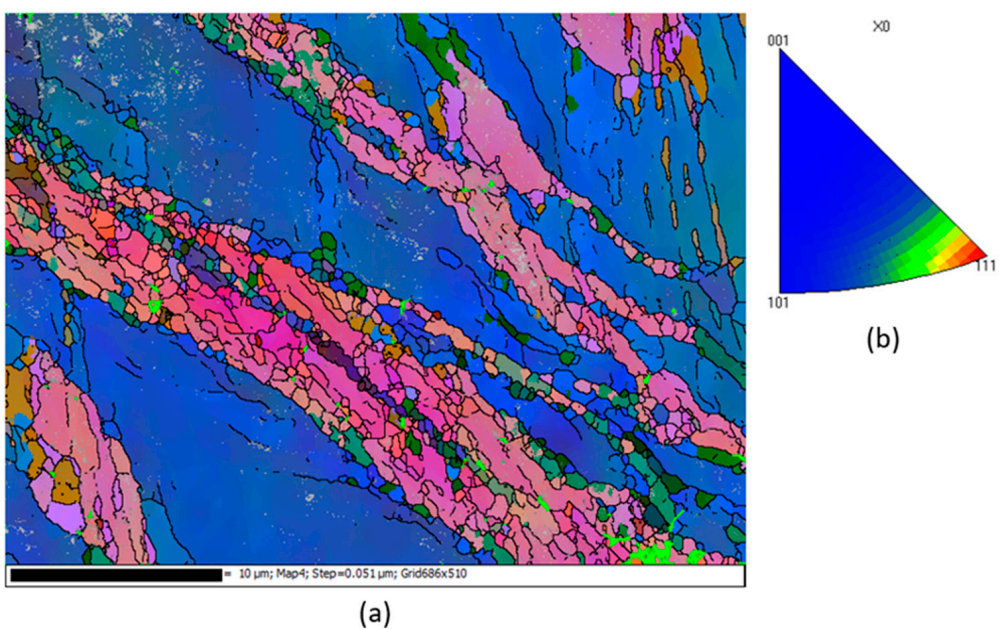


Figure 4. EBSD map of the longitudinal section of the Ti-25Ta-25Nb-3Sn alloy after 2 ECAP passes showing (a) elongated coarse grains around a fine-grained area and (b) the inverse pole figure of the same region.

The constituent phases were investigated using XRD analysis, and the patterns are shown in Figure 6. The thermomechanical characteristics of the ECAP processing have led to the formation of a metastable α'' phase during the first two passes. After four passes, the structure was composed only of β phase, without the presence of α'' phase, as can be seen in Figure 6. The ECAP processing at 500°C has presented sufficient heating and pressure conditions for a tension-induced transformation. Bertrand et al. (2013) studied the $\beta \rightarrow \alpha''$ martensitic transformation on the Ti25Ta25Nb alloy using dynamic mechanical analysis

(DMA) under heating and cooling conditions, the authors observed that during the heating of the material, the martensitic transformation was facilitated [22].

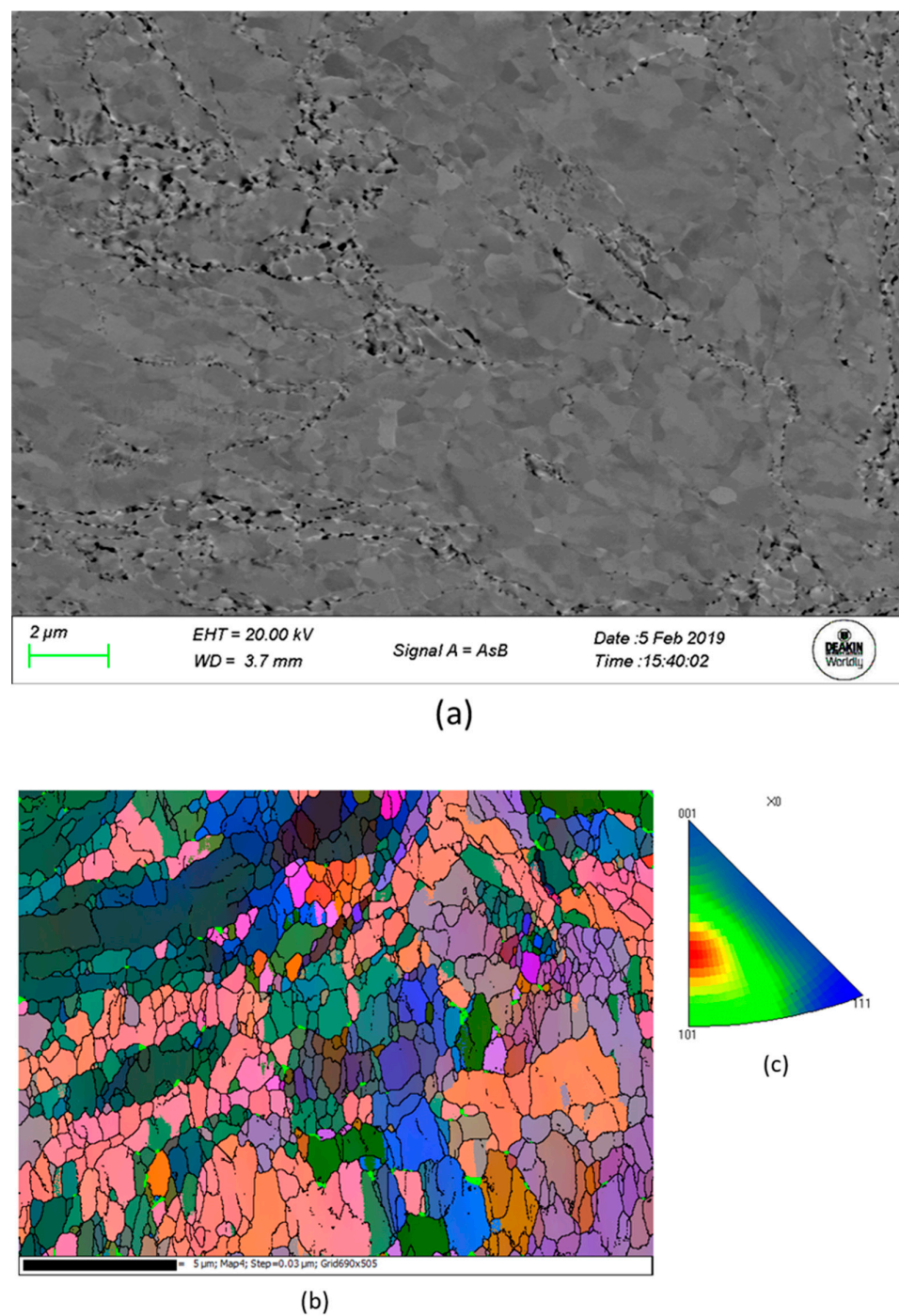


Figure 5. (a) SEM image of the Ti-25Ta-25Nb-3Sn alloy after 4 ECAP passes and (b) EBSD map of the Ti-25Ta-25Nb-3Sn alloy after 4 ECAP passes showing a fine-grained area (c) the inverse pole figure of the same area.

Graph XRD1

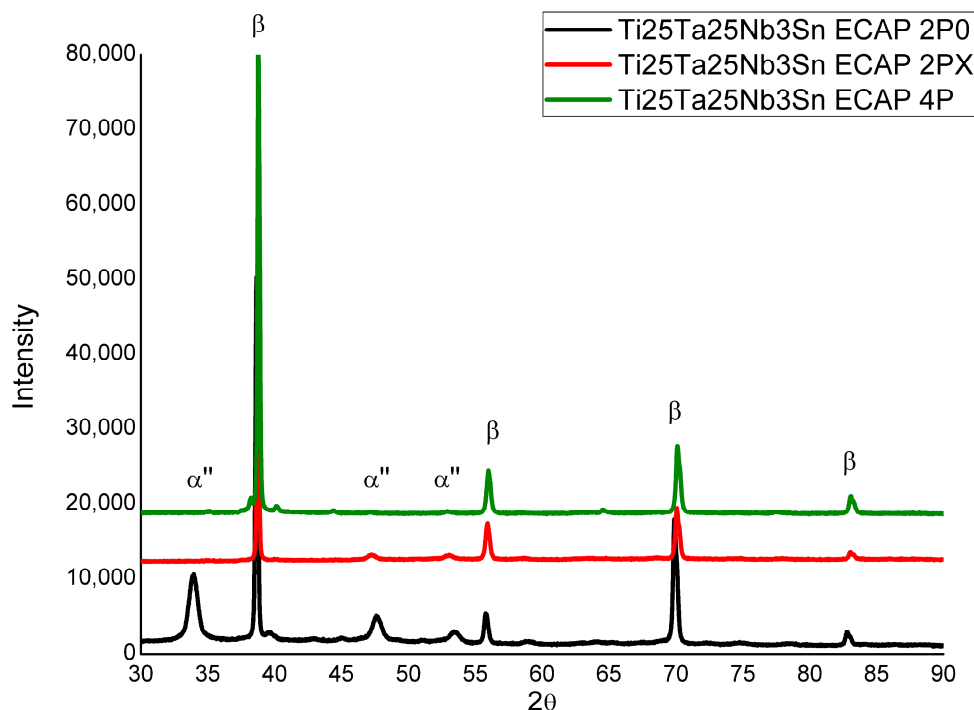


Figure 6. XRD patterns of the Ti-25Ta-25Nb-3Sn after ECAP processing, showing the constituent phases after 2 and 4 passes.

Microhardness tests indicate a slight increase after four ECAP passes, from 193 HV to 212 HV, which is related to the grain size reduction. The obtained results are shown in Table 1.

Table 1. Microhardness measurements after ECAP Processing (2 and 4 passes).

Sample	Microhardness (HV)
As fabricated	193 (3)
ECAP—2 Passes (cross-section)	201 (5)
ECAP—2 Passes (longitudinal section)	201 (4)
ECAP—4 Passes	212 (4)

Formatting of result mean (standard deviation).

The Ti-25Nb-25Ta alloy was previously studied by Seixas et al. (2016) who identified the feasibility of its use in biomedical applications [14,17]. Recently, Silva et al. (2023) verified the effects of adding 5%w of Sn, confirming better results for Ti-25Nb-25Ta-3Sn alloy. In the present work, the alloys processed with ECAP were compared with the cast alloy [18].

The OCP curves (Figure 7a) for the Ti-25Ta-25Nb-3Sn and after ECAP with two passes (Ti-25Ta-25Nb-3Sn ECAP-2) presented a similar behavior without the stabilization of the curves in the recorded range. Initially, the Ti-25Ta-25Nb-3Sn alloy curve showed a short stabilization; however, from 2.5 ks, the registered potential showed a growth ramp. The Ti-25Ta-25Nb-3Sn ECAP-2 material showed a more pronounced growth ramp in relation to the control condition, indicating the formation of oxide layers on the surface of the material during the tests and the high variability of the results. The third group evaluated, Ti-25Ta-25Nb-3Sn ECAP-4, presented a greater stability and homogeneity of results in relation to the other groups. Considering the potential at the end of the test, the Ti-25Ta-25Nb-3Sn ECAP-2 group obtained the best result, followed by the control group and Ti-25Ta-25Nb-3Sn ECAP-4. All groups recorded an open circuit

potential more positive than that found for grade 2 titanium, indicating that both the composition and the mechanical treatment employed, ECAP, resulted in an increase in corrosion resistance.

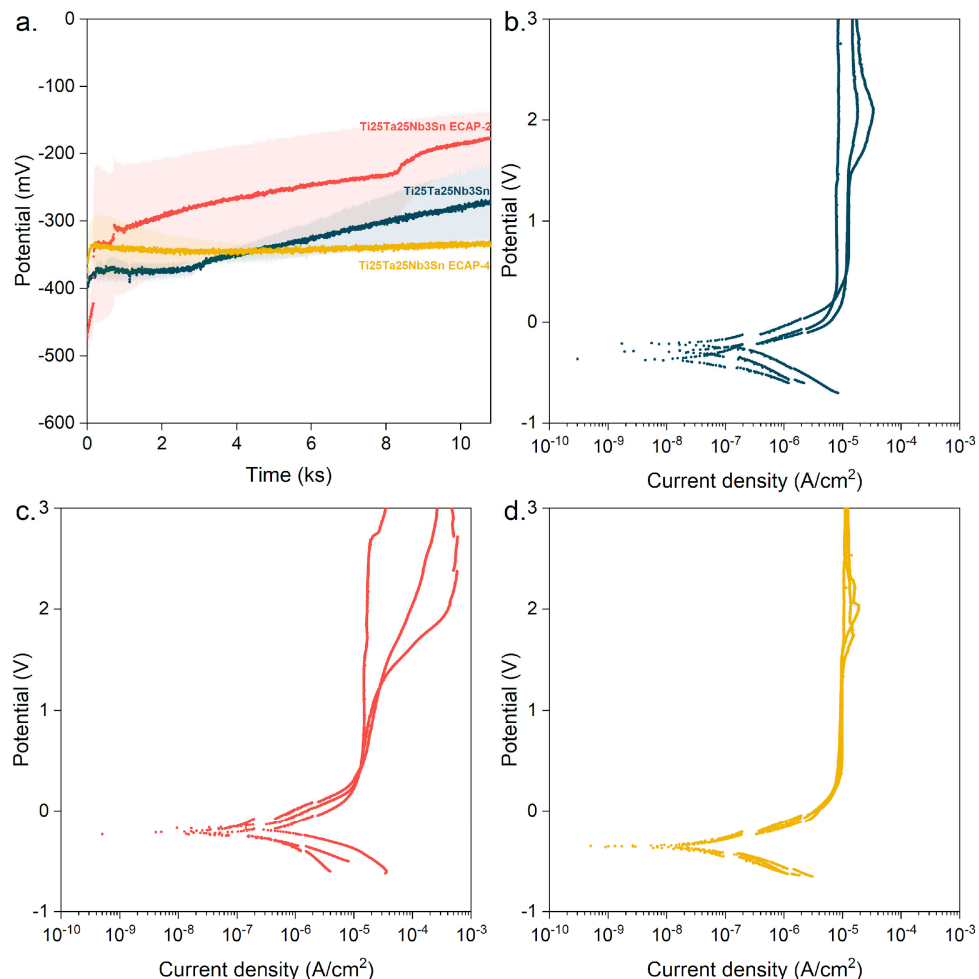


Figure 7. (a) Open circuit potential: average curve and standard deviation obtained from tests on Ti-25Ta-25Nb-3Sn alloy under three processing conditions: as-fabricated and after ECAP with 2 and 4 passes. (b) Potentiodynamic polarization curves obtained for samples of Ti-25Ta-25Nb-3Sn, (c) Ti-25Ta-25Nb-3Sn ECAP-2, and (d) Ti-25Ta-25Nb-3Sn ECAP-4.

Potentiodynamic polarization tests were carried out for a more detailed characterization. The results indicated that the corrosion potential obtained for the three conditions evaluated was close to the value found by the OCP tests, with slightly more positive results. This means that the stabilization of the OCP curve was close to stabilization and the interpretation of this parameter is the same as described earlier. The homogeneity of the results is similar to that observed in OCP, being greater for the Ti-25Ta-25Nb-3Sn ECAP-4 group and lower for the Ti-25Ta-25Nb-3Sn ECAP-2, as can be seen in Figure 7.

It was found that the corrosion density was lower for the Ti-25Ta-25Nb-3Sn ECAP-4 alloy, indicating the better performance of the oxide layer formed on its surface in protecting the material from the action of the fluoride solution. In addition, the increase in the number of passes in the ECAP process had a positive effect on the result, and in all analyzed cases, the corrosion current density was lower than the value found in the literature for grade 2 titanium [19].

The Ti-25Ta-25Nb-3Sn ECAP-4 group presented the best results in relation to the passivation corrosion density (Table 2). A breakdown of the passive layer and repassivation of the material was observed between 1.5 V and 2.5 V (Figure 7d), a behavior similar to that

observed for the Ti-25Ta-25Nb-3Sn alloy (Figure 7b), but with less intensity. The Ti-25Ta-25Nb-3Sn ECAP-2 group showed a greater variation in passivation capacity (Figure 7c), with the formation of a stable passive layer in one of the tests, breakdown, and repassivation in another, and the absence of stabilization of the curve in relation to the current density in a third test, indicating the formation of an unstable passive film.

Table 2. The corrosion parameters obtained for the Ti-25Ta-25Nb-3Sn alloy under three processing conditions, including as-fabricated and after ECAP with 2 and 4 passes, were evaluated. The open-circuit potential (OCP) and potentiodynamic polarization were performed in a fluoride-containing physiological solution (0.15 M NaCl + 0.03 M NaF, pH = 6.0) at 37 °C. (*) Literature data [19] are also included.

Sample	E _{OC} (mV)	E _{corr} (mV)	J _{corr} (nA·cm ⁻²)	J _p (μA·cm ⁻²)
Ti25Ta25Nb3Sn	−277 (64.4)	−283 (60.4)	12.2 (1.8)	10.9 (1.9)
Ti25Ta25Nb3Sn ECAP-2	−178 (67.9)	−206 (28.0)	6.7 (2.2)	14.5
Ti25Ta25Nb3Sn ECAP-4	−337 (14.4)	−353 (4.0)	3.7 (1.1)	9.28 (0.5)
Ti (grade 02) *	−383 *	−376 *	37.4 *	28.0 *

Formatting of results mean (standard deviation).

Based on the results obtained in this research and comparing them with the literature [19], it was found that the alloy composition and the mechanical processing applied resulted in an increase in corrosion resistance compared to grade 2 titanium. The alloying elements, Ta and Nb, exhibit high corrosion resistance, superior to titanium itself, contributing to the increased strength of the Ti-25Ta-25Nb-3Sn alloy [3,14,17,35,36]. On the other hand, Sn leads to the formation of a less stable oxide, acting against the effect of Ta and Nb [19,23,35,36]. However, Sn promotes an increase in the ductility of the alloy [1,25,26,35,36], which facilitates the ECAP process and, consequently, the refinement of the microstructure [9]. The formation of nanosized grains results in an increase in the chemical activity of the material due to the increase in grain boundary density, causing an even faster formation of a stable oxide layer on the surface of the alloy, increasing corrosion resistance, as observed in the Ti-25Ta-25Nb-3Sn alloy after four passes of ECAP [37]. However, a minimum number of passes is necessary for the formation of a homogeneous microstructure, which is reflected in the properties of the alloy.

Therefore, the electrochemical tests carried out in this study indicate that the new Ti25Ta235Nb3Sn alloy exhibits higher corrosion resistance than grade 2 titanium, which is a material commonly used as a reference in the biomedical field. In addition, the ECAP resulted in an increase in chemical stability. These results suggest a potential for application in the biomedical field.

4. Conclusions

The Ti-25Ta-25Nb-3Sn alloy was subjected to ECAP processing to produce an ultrafine-grained structure. After four passes, the microstructure had an average grain diameter of 395 nm, a reduction of about 50%; however, the microstructure was non-homogeneous, which was reflected as a slight increase in the microhardness from 193 to 212 HV. The grain size reduction had a positive outcome, as the corrosion resistance also demonstrated an overall increase after ECAP processing, showing the best results in relation to the passivation corrosion density and an increase in chemical stability. The results suggest that the Ti-25Ta-25Nb-3Sn alloy after ECAP processing may have the potential to be used in biomedical applications; however, the influence of more ECAP passes will be investigated in future studies.

Author Contributions: Conceptualization, C.B.J., A.C.F., I.T. and A.P.R.A.; Methodology, C.B.J., J.P.A.C., A.C.F., I.T. and A.P.R.A.; Formal analysis, C.B.J. and J.P.A.C.; Investigation, C.B.J., A.C.F., I.T. and A.P.R.A.; Data curation, C.B.J., J.P.A.C. and A.P.R.A.; Writing—original draft, C.B.J. and J.P.A.C.; Writing—review and editing, C.B.J., J.P.A.C., A.C.F., I.T. and A.P.R.A.; Visualization, C.B.J. and J.P.A.C.; Supervision, A.P.R.A.; Funding acquisition, I.T. and A.P.R.A. All authors have read and agreed to the published version of the manuscript.

Funding: This study was financed in part by the Coordenação de Aperfeiçoamento de Pessoal de Nível Superior-Brasil (CAPES)-Finance Code 001 and the National Council for Scientific and Technological Development (CNPq) (309469/2015-5) and Unesp—São Paulo State University-Scholarship. The present work was carried out with the support of the Deakin Advanced Characterization Facility.

Data Availability Statement: All data produced during this study is stored in Deakin University's and São Paulo State University's servers.

Conflicts of Interest: The authors declare no conflict of interest.

References

1. Khrunyk, Y.Y.; Ehnert, S.; Grib, S.V.; Illarionov, A.G.; Stepanov, S.I.; Popov, A.A.; Ryzhkov, M.A.; Belikov, S.V.; Xu, Z.; Rupp, F.; et al. Synthesis and characterization of a novel biocompatible alloy, ti-nb-zr-ta-sn. *Int. J. Mol. Sci.* **2021**, *22*, 10611–10630. [[CrossRef](#)] [[PubMed](#)]
2. Su, B.; Wang, B.; Luo, L.; Wang, L.; Su, Y.; Xu, Y.; Wang, F.; Han, B.; Huang, H.; Guo, J.; et al. Effect of zirconium content on the microstructure and corrosion behavior of as-cast Ti-Al-Nb-Zr-Mo alloy. *J. Mater. Res. Technol.* **2019**, *15*, 4896–4913. [[CrossRef](#)]
3. Carobolante, J.P.A.; Pereira Júnior, A.; Bortolini Junior, C.; Barboza da Silva, K.; Sabino, R.M.; Popat, K.C.; Claro, A.P.R.A. Processing and Characterization of a New Quaternary Alloy Ti10Mo8Nb6Zr for Potential Biomedical Applications. *Materials* **2022**, *15*, 8636–8653. [[CrossRef](#)]
4. Cardoso, G.C.; de Almeida, G.S.; Corrêa, D.O.G.; Zambuzzi, W.F.; Buzalaf, M.A.R.; Correa, D.R.N.; Grandini, C.R. Preparation and characterization of novel as-cast Ti-Mo-Nb alloys for biomedical applications. *Sci. Rep.* **2022**, *12*, 11874. [[CrossRef](#)] [[PubMed](#)]
5. Kaur, M.; Singh, K. Review on titanium and titanium based alloys as biomaterials for orthopaedic applications. *Mater. Sci. Eng. C* **2019**, *102*, 844–862. [[CrossRef](#)] [[PubMed](#)]
6. Zhang, L.; Chen, L. A Review on Biomedical Titanium Alloys: Recent Progress and Prospect. *Adv. Eng. Mater.* **2019**, *21*, 1801215. [[CrossRef](#)]
7. Carobolante, J.P.A.; Pereira, C.A.; Dias-Netipanyj, M.F.; Popat, K.C.; Claro, A.P.R. Cell and bacteria-Baterial interactions on the Ti10Mo8Nb alloy after surface modification. *Mater. Res.* **2018**, *21*, e20170508. [[CrossRef](#)]
8. Carobolante, J.P.A.; da Silva, K.B.; Chaves, J.A.M.; Dias Netipanyj, M.F.; Popat, K.C.; Alves Claro, A.P.R. Nanoporous layer formation on the Ti10Mo8Nb alloy surface using anodic oxidation. *Surf. Coat. Technol.* **2020**, *386*, 125467–125476. [[CrossRef](#)]
9. Churakova, A.A.; Gunderov, D.V.; Raab, G.I.; Prokoshkin, S.D.; Sheremetev, V.A.; Filho, P.N.L.; Pedro, J.; Claro, A.P.R.A. Influence of ECAP on the structure and properties of Ti18Zr15Nb and Ti10Mo8Nb6Zr alloys for medical application. *IOP Conf. Ser. Mater. Sci. Eng.* **2021**, *1014*, 012006–012010. [[CrossRef](#)]
10. Takahashi, M.; Kikuchi, M.; Takada, Y. Mechanical properties and microstructures of dental cast Ti-6Nb-4Cu, Ti-18Nb-2Cu, and Ti-24Nb-1Cu alloys. *Dent. Mater. J.* **2016**, *35*, 564–570. [[CrossRef](#)]
11. Ozan, S.; Lin, J.; Li, Y.; Zhang, Y.; Munir, K.; Jiang, H.; Wen, C. Deformation mechanism and mechanical properties of a thermomechanically processed β Ti-28Nb-35.4 Zr alloy. *J. Mech. Behav. Biomed. Mater.* **2018**, *78*, 224–234. [[CrossRef](#)]
12. Yamako, G.; Janssen, D.; Hanada, S.; Anijs, T.; Ochiai, K.; Totoribe, K.; Chosa, E.; Verdonschot, N. Improving stress shielding following total hip arthroplasty by using a femoral stem made of β type Ti-33.6Nb-4Sn with a Young's modulus gradation. *J. Biomech.* **2017**, *63*, 135–143. [[CrossRef](#)]
13. Keshtta, A.; Gepreel, M.A.H. Superelasticity evaluation of the biocompatible Ti-17Nb-6Ta alloy. *J. Healthc. Eng.* **2019**, *2019*, 8353409. [[CrossRef](#)]
14. Seixas, M.R.; Bortolini, C., Jr.; Konatu, R.T.; Pereira, A., Jr.; Rosifini Alves Claro, A.P. Mechanical and microstructural characterization of the Ti-25Ta-25Nb alloy for dental applications. *Mater. Sci. Forum* **2016**, *869*, 935–939. [[CrossRef](#)]
15. Zhan, H.; Zeng, W.; Wang, G.; Kent, D.; Dargusch, M. On the deformation mechanisms and strain rate sensitivity of a metastable β Ti-Nb alloy. *Scr. Mater.* **2015**, *107*, 34–37. [[CrossRef](#)]
16. Liu, H.; Yang, J.; Zhao, X.; Sheng, Y.; Li, W.; Chang, C.-L.; Zhang, Q.; Yu, Z.; Wang, X. Microstructure, mechanical properties and corrosion behaviors of biomedical Ti-Zr-Mo-xMn alloys for dental application. *Corros. Sci.* **2019**, *161*, 108195. [[CrossRef](#)]
17. Seixas, M.R.; Bortolini, C.; Pereira, A.; Nakazato, R.Z.; Popat, K.C.; Alves Claro, A.P.R. Development of a new quaternary alloy Ti-25Ta-25Nb-3Sn for biomedical applications. *Mater. Res. Express* **2018**, *5*, 025402. [[CrossRef](#)]
18. Silva, K.B.D.; Carobolante, J.P.A.; Rajan, S.S.; Júnior, C.B.; Sabino, R.M.; Seixas, M.R.; Nakazato, R.Z.; Popat, K.C.; Claro, A.P.R.A. Mechanical Properties, Corrosion Behavior, and In Vitro Cell Studies of the New Ti-25Ta-25Nb-5Sn Alloy. *Materials* **2023**, *16*, 1970. [[CrossRef](#)]

19. Zhou, Y.L.; Niinomi, M.; Akahori, T. Effects of Ta content on Young's modulus and tensile properties of binary Ti-Ta alloys for biomedical applications. *Mater. Sci. Eng. A* **2004**, *371*, 283–290. [[CrossRef](#)]
20. Wang, C.H.; Liu, M.; Hu, P.F.; Peng, J.C.; Wang, J.A.; Ren, Z.M.; Cao, G.H. The effects of α'' and ω phases on the superelasticity and shape memory effect of binary Ti-Mo alloys. *J. Alloys Compd.* **2017**, *720*, 488–496. [[CrossRef](#)]
21. Bertrand, E.; Gloriant, T.; Gordin, D.M.; Vasilescu, E.; Drob, P.; Vasilescu, C.; Drob, S.I. Synthesis and characterisation of a new superelastic Ti-25Ta-25Nb biomedical alloy. *J. Mech. Behav. Biomed. Mater.* **2010**, *3*, 559–564. [[CrossRef](#)]
22. Bertrand, E.; Castany, P.; Gloriant, T. Investigation of the martensitic transformation and the damping behavior of a superelastic Ti-Ta-Nb alloy. *Acta Mater.* **2013**, *61*, 511–518. [[CrossRef](#)]
23. Li, S.J.; Cui, T.C.; Hao, Y.L.; Yang, R. Fatigue properties of a metastable β -type titanium alloy with reversible phase transformation. *Acta Biomater.* **2008**, *4*, 305–317. [[CrossRef](#)]
24. Ma, B.; Ju, D.; Liu, Q. Design, Simulation and Performance Research of New Biomaterial Mg₃₀Zn₃₀Sn₃₀Sr₅Bi₅. *Coatings* **2022**, *12*, 531. [[CrossRef](#)]
25. Da Silva Dias, C.; Rossi, M.C.; Apolonio, E.V.P.; dos Santos Rosa, G.; Pfeifer, J.P.H.; Hussni, C.A.; Watanabe, M.J.; Alves, A.L.G. Low Mg content on Ti-Nb-Sn alloy when in contact with eBMMSCs promotes improvement of its biological functions. *J. Mater. Sci. Mater. Med.* **2021**, *32*, 144. [[CrossRef](#)]
26. Çakmak, Ö.; Kaya, M. Effect of sintering procedure on microstructure and mechanical properties of biomedical TiNbSn alloy produced via powder metallurgy. *Appl. Phys. A* **2021**, *127*, 561. [[CrossRef](#)]
27. Edalati, K.; Bachmaier, A.; Beloshenko, V.A.; Beygelzimer, Y.; Blank, V.D.; Botta, W.J.; Bryła, K.; Čížek, J.; Divinski, S.; Enikeev, N.A.; et al. Nanomaterials by severe plastic deformation: Review of historical developments and recent advances. *Mater. Res. Lett.* **2022**, *10*, 163–256. [[CrossRef](#)]
28. Gunderov, D.V.; Polyakov, A.V.; Semenova, I.P.; Raab, G.I.; Churakova, A.A.; Gimaltdinova, E.I.; Sabirov, I.; Segurado, J.; Situdikov, V.D.; Alexandrov, I.V.; et al. Evolution of microstructure, macrotexture and mechanical properties of commercially pure Ti during ECAP-conform processing and drawing. *Mater. Sci. Eng. A* **2013**, *562*, 128–136. [[CrossRef](#)]
29. Polyakov, A.V.; Semenova, I.P.; Huang, Y.; Valiev, R.Z.; Langdon, T.G. Fatigue Life and Failure Characteristics of an Ultrafine-Grained Ti-6Al-4V Alloy Processed by ECAP and Extrusion. *Adv. Eng. Mater.* **2014**, *16*, 1038–1043. [[CrossRef](#)]
30. Terynková, A.; Bartha, K.; Stráský, J.; Janeček, M.; Landa, M.; Polyakova, V.; Semenova, I. Microstructure and mechanical properties of Ti15Mo alloy prepared by ECAP. *Acta Phys. Pol. A* **2018**, *134*, 787–789. [[CrossRef](#)]
31. Semenova, I.P.; Polyakov, A.V.; Polyakova, V.V.; Grishina, Y.F.; Huang, Y.; Valiev, R.Z.; Langdon, T.G. Mechanical behavior and impact toughness of the ultrafine-grained Grade 5 Ti alloy processed by ECAP. *Mater. Sci. Eng. A* **2017**, *696*, 166–173. [[CrossRef](#)]
32. Xu, H.Q.; Wei, K.X.; Wei, W.; Dzugan, J.; Alexandrov, I.V.; An, X.L.; Wang, D.D.; Liu, X.K.; Daniel, M.; Hradil, D.; et al. Microstructure and mechanical properties evolution of Ti-13Nb-13Zr alloy processed by ECAP-Conform and rotary swaging. *J. Alloys Compd.* **2023**, *969*, 172351. [[CrossRef](#)]
33. Munir, K.; Lin, J.; Wright, P.F.; Ozan, S.; Li, Y.; Wen, C. Mechanical, corrosion, nanotribological, and biocompatibility properties of equal channel angular pressed Ti-28Nb-35.4 Zr alloys for biomedical applications. *Acta Biomater.* **2022**, *149*, 387–398. [[CrossRef](#)]
34. Valiev, R.Z.; Prokofiev, E.A.; Kazarinov, N.A.; Raab, G.I.; Minasov, T.B.; Stráský, J. Developing nanostructured Ti alloys for innovative implantable medical devices. *Materials* **2020**, *13*, 967–983. [[CrossRef](#)]
35. Wang, Z.; Yan, Y.; Wu, Y.; Huang, X.; Zhang, Y.; Su, Y.; Qiao, L. Corrosion and tribocorrosion behavior of equiatomic refractory medium entropy TiZr (Hf, Ta, Nb) alloys in chloride solutions. *Corros. Sci.* **2022**, *199*, 110166. [[CrossRef](#)]
36. Khan, H.M.; Özer, G.; Yilmaz, M.S.; Koc, E. Corrosion of additively manufactured metallic components: A review. *Arab. J. Sci. Eng.* **2022**, *47*, 5465–5490. [[CrossRef](#)]
37. Motyka, M. Martensite formation and decomposition during traditional and AM processing of two-phase titanium alloys—An overview. *Metals* **2021**, *11*, 481–498. [[CrossRef](#)]

Disclaimer/Publisher's Note: The statements, opinions and data contained in all publications are solely those of the individual author(s) and contributor(s) and not of MDPI and/or the editor(s). MDPI and/or the editor(s) disclaim responsibility for any injury to people or property resulting from any ideas, methods, instructions or products referred to in the content.